Published online 6 October 2021 *Nucleic Acids Research, 2021, Vol. 49, No. 19* **11211–11223**
https://doi.org/10.1093/nar/gkab874

Single-molecule conformational dynamics of a transcription factor reveals a continuum of binding modes controlling association and dissociation

Wei Chen [1], Wei Lu [2], Peter G. Wolynes [2] and Elizabeth A. Komives [1,*]

[1]Department of Chemistry and Biochemistry, University of California San Diego, La Jolla, California 92093, USA and [2]Center for Theoretical Biological Physics, Departments of Chemistry, Physics, and Biosciences, Rice University, Houston, Texas 77005, USA

Received June 11, 2021; Revised September 10, 2021; Editorial Decision September 13, 2021; Accepted September 22, 2021

ABSTRACT

Binding and unbinding of transcription factors to DNA are kinetically controlled to regulate the transcriptional outcome. Control of the release of the transcription factor NF-κB from DNA is achieved through accelerated dissociation by the inhibitor protein IκBα. Using single-molecule FRET, we observed a continuum of conformations of NF-κB in free and DNA-bound states interconverting on the subseconds to minutes timescale, comparable to *in vivo* binding on the seconds timescale, suggesting that structural dynamics directly control binding kinetics. Much of the DNA-bound NF-κB is partially bound, allowing IκBα invasion to facilitate DNA dissociation. IκBα induces a locked conformation where the DNA-binding domains of NF-κB are too far apart to bind DNA, whereas a loss-of-function IκBα mutant retains the NF-κB conformational ensemble. Overall, our results suggest a novel mechanism with a continuum of binding modes for controlling association and dissociation of transcription factors.

INTRODUCTION

Eukaryotic gene expression starts with a transcription factor binding to a specific DNA sequence. After recognizing the DNA, the transcription factor recruits co-activators and eventually RNA polymerase to transcribe DNA to RNA messages (1). Transcription occurs as irregular bursts, and the burst frequency and size determine the gene expression level (2–6). Live-cell imaging revealed that the burst frequency is controlled by the bound fraction of the transcription factor and the burst size is determined by the transcription factor dwell time (7). Bursts continue as long as the transcription factor stays bound and they terminate once the transcription factor dissociates from DNA (8). In other words, the rates of association (on rate) and dissociation (off rate) of the transcription factor to and from the DNA are critical in determining the amount of RNA produced (9). Overall, transcriptional regulation is likely under kinetic control (3,5,10–12), where the on and off rates of macromolecular interactions are finely tuned, as opposed to thermodynamic control (13,14), where everything is governed by equilibrium constants. It is therefore important to understand the molecular mechanism behind the control of the on and off rates of transcription factors.

Recent single-molecule tracking of diffusion and binding of several transcription factors in live cells suggested that the off rate (the inverse of dwell time on DNA) follows a continuous distribution (15,16), instead of only two discrete populations corresponding to specifically and non-specifically bound as implied by decades of biochemical studies (17). A continuum of off rates was only found in transcription factors containing intrinsically disorder regions (IDRs), and removal of the IDR resulted in two discrete populations (15). It remains unknown whether the broad distribution of off rates reflects the heterogeneous nuclear environment or is an intrinsic kinetic property of the protein–DNA complex (15,16). Yet the essential role of the IDRs suggests that the continuous distribution of off rates may originate from structural heterogeneity in the bound complex.

Controlling the off rate of a transcription factor may seem improbable if it depends on spontaneous dissociation from DNA, in which a higher off rate means fewer contacts and thus less specificity in the protein-DNA complex. Several DNA-binding proteins have been shown to dissociate more readily in the presence of increasing concentrations of the protein itself (18–23). The mechanism of this 'facilitated dissociation' involves the formation of a transient ternary complex in which two DNA-binding proteins are each bound to part of the DNA binding site (24). For the transcription factor NF-κB, a third player, the inhibitor protein IκBα was shown to facilitate dissociation of NF-κB from DNA in a process later termed molecular stripping (10,25). In this case, a transient IκBα/NF-κB/DNA

*To whom correspondence should be addressed. Tel: +1 858 534 3058; Email: ekomives@ucsd.edu

ternary complex is formed, and the off rate is proportional to the IκBα concentration (25,26). Molecular stripping enables tuning of the off rate without sacrificing the binding affinity and offers a clean termination of transcription by fast removal of transcription factors on demand (27). Similar processes have also been observed in other systems. For example, prothymosin α can remove histone H1 from nucleosomes (28) and the negative regulator, CITED2 displaces the HIF-1α C-terminal domain from the TAZ1 domain of CBP/p300 (29).

A mechanistic understanding of kinetic control, including molecular stripping and the distribution of *in vivo* off rates, demands a deeper understanding of the protein conformational dynamics. To investigate the structural origin of kinetic control for protein-DNA interactions, we carried out single-molecule FRET (smFRET) experiments to visualize the conformational dynamics of NF-κB in real time. Our results presented here reveal a continuum of conformations of NF-κB in both free and DNA-bound states. These conformations interconvert on a range of timescales from hundreds of milliseconds to minutes, comparable to *in vivo* binding events on the seconds timescale (30), and suggest a structural explanation for the *in vivo* off rate distribution and a binding mechanism utilizing a continuum of binding modes for DNA association and molecular stripping.

Here NF-κB refers to the heterodimer formed by the Rel homology domains of subunits RelA (also known as p65) and p50. Each subunit consists of a dimerization domain (DD) and an N-terminal DNA-binding domain (NTD) connected by a 10-amino acid linker. NF-κB recognizes DNA with its two NTDs (Figure 1A), which can undergo nanoscale interdomain motions to expose or occlude the DNA-binding cavity as shown by hydrogen-deuterium exchange experiments, molecule dynamics (MD) simulations and stopped-flow fluorescence experiments (31). NF-κB activates transcription in response to extracellular stimuli, and is otherwise held inactive in the cytoplasm by the inhibitor protein, IκBα (32) (Figure 1B). NF-κB can shuttle between the cytosol and the nucleus (33–35). Upon stimulation, targeted degradation of IκBα (36) exposes the nuclear localization signal of NF-κB, allowing NF-κB translocation to the nucleus where it binds DNA (37). NF-κB activates hundreds of genes, including the one of its own inhibitor, IκBα, therefore creating a negative feedback loop (38–40): the newly synthesized IκBα enters the nucleus (41), strips NF-κB from DNA (10,25–27), prevents DNA rebinding and returns the NF-κB/IκBα complex to the cytoplasm to terminate the transcriptional response (27,41) (Figure 1C). Molecular stripping of NF-κB starts with IκBα encountering DNA-bound NF-κB followed by the formation of a transient IκBα/NF-κB/DNA ternary complex (10,26). MD simulations showed that IκBα induces a twist in the NTDs so that DNA is only held by one NTD, and thus lowers the barrier for dissociation (10). An IκBα mutant capable of binding to NF-κB but unable to strip leads to slower export of NF-κB from the nucleus in live cells (27), indicating that molecular stripping is critical for efficient termination of the transcriptional response.

Here we report a remarkable observation of a continuum of conformations of NF-κB in the free and DNA-bound states by monitoring the real-time interdomain motions of

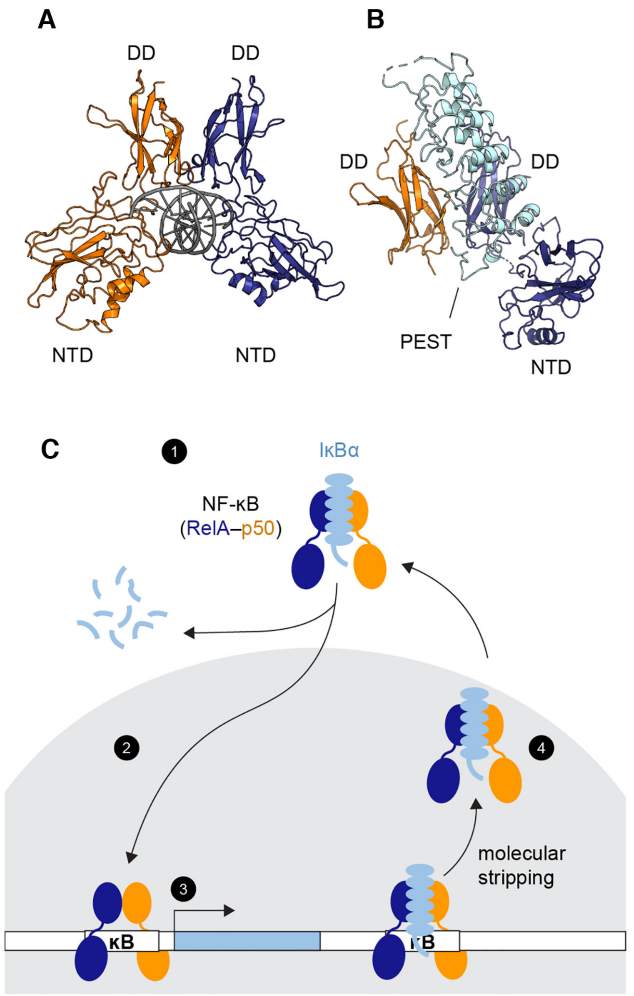

Figure 1. Transcriptional regulation by NF-κB. (**A**) Structure of the NF-κB RelA-p50 heterodimer bound to DNA (PDB: 1LE5, RelA in blue, p50 in orange and DNA in gray). Each monomer contains a dimerization domain (DD) and an N-terminal DNA binding domain (NTD) connected by a 10-amino-acid linker. The NF-κB dimer recognizes its cognate DNA through the two NTDs (**B**) Structure of the NF-κB bound to the inhibitor protein IκBα (PDB: 1IKN, IκBα in cyan). IκBα binds to the DDs of NF-κB. The disordered PEST sequence of IκBα inserts into the DNA-binding cavity. The NTD of p50 was truncated to achieve crystallization. (**C**) Schematic of NF-κB transcriptional regulation showing (1) NF-κB is held inactive in the cytoplasm by IκBα. (2) Upon stimulation, targeted degradation of IκBα allows free NF-κB to translocate to the nucleus (gray). (3) NF-κB binds DNA and activates genes including the one of IκBα, creating newly synthesized IκBα. (4) IκBα enters the nucleus, accelerates the dissociation of NF-κB from the DNA via molecular stripping, and returns NF-κB to the cytoplasm.

the NTDs. The broad conformational distribution of DNA-bound NF-κB provides a possible structural explanation of the off rate distribution of transcription factors in live cells (15,16) and a mechanistic understanding of molecular stripping, where the broad conformational distribution containing partially unbound states would allow IκBα to invade the DNA-binding cavity of NF-κB and accelerate DNA dissociation. We found that IκBα induces a single static conformation in NF-κB where the DNA-binding domains are too far apart to both bind DNA, explaining how it accelerates

DNA dissociation and inhibits DNA binding (25–27). A stripping impaired IκBα mutant still allows the interdomain motions in NF-κB, some of which permit DNA binding. Overall, our results suggest a novel mechanism of macromolecular interactions by utilizing a continuum of binding modes in both association and dissociation to allow kinetic control. It is also the first time that a continuum of conformations connected by extremely slow motions is directly resolved and visualized, revealing a highly rugged energy landscape and its biological function.

MATERIALS AND METHODS

Protein expression, purification, and labeling

Plasmids of murine $RelA_{1–325}$ (UniProt entry Q04207) and $p50_{39–363}$ (UniProt entry P25799) in pET11a vectors (Plasmid #44744, Addgene) were provided by Gourisankar Ghosh at UCSD. A 6xHis-tag for immobilization was introduced to the C-terminus of RelA by site-directed mutagenesis. We previously determined a K_D of 6.7 nM for untagged RelA-p50 binding to the IFN DNA by surface plasmon resonance, and a K_D of 2.8 nM for RelA-p50 with a His-tag on the N-terminal domain of p50 binding to the IFN DNA by stopped-flow fluorescence (25,26). The C-terminal His-tag in this study is far from the N-terminal DNA-binding domains and therefore does not interfere with binding. Q128 of RelA and F148 of p50 were mutated into Amber stop codons TAG by site-directed mutagenesis for unnatural amino acid incorporation and fluorophore labeling. Plasmid containing RelA or p50 was co-transformed with pEVOL-pAzF (Plasmid #31186, Addgene), the plasmid encoding the aaRS/tRNA pair for incorporating the unnatural amino acid p-azidophenylalanine (pAzF, CAS 33173-53-4, Chem-Impex Int'l. Inc.), into BL21 (DE3) *E. coli* strain (New England Biolabs). Cells were grown in M9 minimal media with 200 mg/L ampicillin and 34 mg/L chloramphenicol at 37°C and 180 rpm. At 0.6–0.7 OD_{600}, the expression of RelA or p50 was induced with 0.2 mM IPTG, and the expression of the aaRS/tRNA was induced with 0.02% L-arabinose. pAzF was added to a 200 mg/L final concentration. Cells were then grown at 18°C and 180 rpm for 16 h and harvested by centrifugation at 5000 rcf for 15 min. The cell pellet containing His-tagged RelA was resuspended in 50 mM sodium phosphate pH 8, 150 mM NaCl, 10 mM imidazole, 0.5 mM PMSF with protease inhibitor cocktail (Sigma-Aldrich). Following sonication on ice, the cell lysate was centrifuged at 17,000 rcf for 30 min. The supernatant was passed through Ni-NTA resins (Thermo Fisher Scientific) and washed with 10 column volumes of the wash buffer (50 mM sodium phosphate pH 8, 150 mM NaCl, 20 mM imidazole). RelA was eluted with 50 mM sodium phosphate pH 8, 150 mM NaCl, 250 mM imidazole. The eluent was passed through a PD-10 desalting column (GE Healthcare) equilibrated with with 25 mM Tris pH 7.5, 150 mM NaCl, 0.5 mM EDTA to remove imidazole. After addition of the protease inhibitor cocktail and glycerol (5% final concentration), the sample was aliquoted and stored at −80°C for further fluorophore labeling and purification. The cell pellet containing non-tagged RelA or p50 was resuspended in 25 mM Tris pH 7.5, 150 mM NaCl, 0.5 mM EDTA, 0.5 mM PMSF. After sonication and centrifugation, the supernatant was passed through SP Sepharose Fast Flow resins (GE Healthcare). The protein was eluted with a gradient of 0–700 mM NaCl. The elution fraction was purified with a PD-10 desalting column and stored in 20 mM Tris pH 7.5, 150 mM NaCl, 0.5 mM EDTA, 5% glycerol at −80°C. Reducing agents were avoided to prevent reducing pAzF to pAmF (p-aminophenylalanine). Expression of full-length $RelA_{1–325}$ and $p50_{39–363}$ was confirmed by SDS-PAGE.

Site-specific incorporation of pAzF was confirmed by pepsin digestion and tandem mass spectrometry, which showed peptides DLE*AISQR (MH+ 1093.567, residues 126–133 of RelA) and GILHVTKKKV*ETL (MH+ 1653.984, residues 138–161 of p50) containing pAzF (denoted by asterisk). Fluorophore labeling was achieved through the copper-free click reaction between the azido sidechain of the incorporated pAzF and the sDIBO functional group on the fluorophore. RelA and p50 were thawed from −80°C and labeled separately with Click-iT™ Alexa Fluor™ 555 sDIBO Alkyne (FRET donor, Thermo Fisher Scientific) or Click-iT™ Alexa Fluor™ 647 sDIBO Alkyne (FRET acceptor, Thermo Fisher Scientific) with a 1:2 protein-to-dye molar ratio at 4°C for 2–7 days. Excess dyes were removed with PD-10 desalting columns. Labeling efficiency was determined by UV-Vis absorbance with the extinction coefficients $\varepsilon^{RelA}{}_{280} = 20{,}400\ M^{-1}\ cm^{-1}$, $\varepsilon^{p50}{}_{280} = 23{,}380\ M^{-1}cm^{-1}$, $\varepsilon^{Alexa555}{}_{555} = 155{,}000\ M^{-1}cm^{-1}$, $\varepsilon^{Alexa647}{}_{650} = 239{,}000\ M^{-1}cm^{-1}$ and the correction factors accounting for absorbance at 280 nm from the dyes ($CF_{Alexa555} = 0.08$, $CF_{Alexa657} = 0.03$). The labeling efficiency was 29–56% for Alexa Fluor 555 to RelA, 20–35% for Alexa Fluor 647 to RelA, 52–83% for Alexa Fluor 647 to p50 and 18–50% for Alexa Fluor 647 to p50. Labeled RelA and p50 were mixed with a 1:5 donor:acceptor molar ratio to form RelA-p50 heterodimer. The dual-labeled heterodimer was then purified by cation exchange chromatography (Mono S 10/100, GE Healthcare) in 25 mM Tris pH 7.5, 0.5 mM EDTA, 1 mM DTT with an NaCl gradient from 100–700 mM and size exclusion chromatography (Superdex 200, GE Healthcare) in Tris pH 7.5, 150 mM NaCl, 0.5 mM EDTA, 1 mM DTT as previously used for wild-type RelA-p50 heterodimer (25). The FRET radius (R_0) of the Alexa Fluor 555/647 pair is 51 Å.

Human $I\kappa B\alpha_{67–287}$ (Uniprot entry P25963) in pET11a was introduced with a N-terminal 6xHis tag. The 5xPEST IκBα had the following mutations: E282Q/E284Q/D285N/E286Q/E287Q and was expressed and harvested as previously described for nontagged IκBα (42). Cell lysates were passed through Ni-NTA resin equilibrated in 25 mM Tris pH 7.5, 150 mM NaCl, 10 mM imidazole, 10 mM βME, washed with 25 mM Tris pH 7.5, 150 mM NaCl, 20 mM imidazole, 10 mM βME and eluted with 25 mM Tris pH 7.5, 150 mM NaCl, 250 mM imizadole, 10 mM βME. Fractions containing IκBα were then dialysed overnight at 4°C in SEC buffer containing 25 mM Tris pH 7.5, 150 mM NaCl, 0.5 mM EDTA, 1 mM DTT. The dialyzed protein was then either frozen in 2 ml aliquots at −80°C until needed or immediately further purified from aggregates by size exclusion chromatography (Superdex S75; GE Healthcare) in SEC buffer. The

IκBα concentration was determined with the extinction coefficient $\varepsilon^{I\kappa B\alpha}{}_{280} = 12{,}950\ M^{-1}\ cm^{-1}$.

Single-molecule FRET data collection

A prism-type total internal reflection fluorescence (TIRF) microscopy was used (43). For the Alexa Fluor 555/ Alexa Flour 647 dye pair, a 532 nm laser (SAPPHIRE 532–300 CW CDRH, Coherent) and a 637 nm laser (OBIS™ 1196625 | 637nm LX 140mW Laser, Coherent) were set up to excite donor and acceptor respectively. Laser output powers were set to 50 mW for smFRET experiments. 532 nm and 637 nm laser beams were guided by mirrors and a beam splitter to colocalize on the excitation area on the prism. An inverted microscope was set up by mounting the objective (CFI Plan Apochromat VC 60XC WI, Nikon) on a Rapid Automated Modular Microscope System (Applied Scientific Instrumentation). Emission light was further split into donor and acceptor channels with a DV2 Two-Channel, Simultaneous-Imaging System (Photometrics) with band pass filters (ET585/65m for donor channel and ET685/56m for acceptor channel, Chroma). Fluorescent signals were detected by Electron Multiplying Charge-Coupled Device (EMCCD) (iXonEM + EMCCD camera, DU-897E-CS0-#BV, Andor Technology).

The DDS-Tween 20 passivated surface (44) with 0.2 mg/ml biotinylated bovine serum albumin (A8549, Sigma-Aldrich) and 0.2 mg/ml NeutrAvidin (31000, Thermo Fisher Scientific) was used to immobilize NF-κB on the quartz microscope slide. For free NF-κB experiments, NF-κB molecules were immobilized through the 6xHis-tag on the C-terminus of RelA by penta-His antibody biotin conjugate (34440, Qiagen). For DNA-bound NF-κB experiments, DNA/NF-κB complexes were immobilized through the interactions between NeutrAvidin and the biotinylated hairpin DNA containing the underlined κB sequence: Biotin-GCATGCGGGAAATTCCATGCAT GCCCCCCATGCATGGAATTTCCCGCATGC. For IκBα-bound NF-κB experiments, IκBα/NF-κB complexes were immobilized through the 6xHis-tag on the N-terminus of IκBα.

Experiments were performed at room temperature in imaging buffer (25 mM Tris pH 7.5, 150 mM NaCl, 0.5 mM EDTA, 0.8 mg/ml glucose oxidase (G2133, Sigma-Aldrich), 0.2 mg/ml catalase (219001, CALBIOCHEM), 0.4% dextrose, and 5 mM Trolox (CAS 53188-07-1, Sigma-Aldrich)). Trolox was prepare by dissolving 10 mg Trolox powder in 10 mL of 25 mM Tris, pH 7.5, 150 mM NaCl, 0.5 mM EDTA with vortexing for 30 min and incubation at room temperature and ambient light overnight (45). The 637 nm laser was used to confirm the existence of acceptor fluorophores and the 532 nm laser was used for excitation of the donor fluorophore. Data acquisition and analysis software were obtained from the Ha Lab at Johns Hopkins University http://ha.med.jhmi.edu/resources/#1464200861600-0fad9996-bfd4. Single molecule movies were recorded with 100 ms time resolution.

Single-molecule FRET data analysis

Individual single-molecule traces were extracted from the acquired movies with the IDL scripts in the Ha Lab software package. The traces were further selected based on the criteria: (i) clear single photobleaching step for both donor and acceptor; (ii) anticorrelation pattern for donor and acceptor intensities; (iii) stable total fluorescence intensity before photobleaching; (iv) >10 s photobleaching lifetime for both donor and acceptor. Time periods with no signals caused by donor or acceptor dark states, an unbound state, or a state in which an unlabeled NF-κB is bound to the immobilized DNA or IκBα were excluded. For each trace, background was defined as the mean values of the donor and acceptor fluorescence intensities after photobleaching and subtracted from the data. To account for the donor signal leakage to the acceptor channel, we measured the correction factor by collecting data of Alexa Fluor 555 labeled RelA. After background subtraction for individual traces of Alexa Fluor 555 labeled RelA, the correction factor was defined as the mean value of the ratio of the acceptor intensity to the donor intensity and calculated to be 0.04. Therefore, for a single-molecule trace, the background and donor leakage are corrected by the following equation in which I is the fluorescent intensity:

$$I_{donor} = I^{raw}_{donor} - I^{background}_{donor}$$

$$I_{acceptor} = I^{raw}_{acceptor} - I^{background}_{acceptor} - 0.04 \times I_{donor}$$

The FRET efficiency (E) was calculated using the corrected fluorescent intensities. $E = I_{\text{acceptor}} / (I_{\text{donor}} + I_{\text{acceptor}})$. Finally, traces were categorized as fluctuating if the anticorrelated fluctuations of donor and acceptor signals were larger than that caused by noise (shown in the signal after photobleaching). Traces with no fluctuations larger than noise were categorized as stable.

FRET data were presented in two types of histograms. In the first type, the first 1000 timepoints (10 seconds) of each trace were used as data points to build the histogram. In the second type, mean FRET efficiency values of each individual long-lived state were used as data points to build the histogram. The first type of histogram built by counting timepoints is useful for general purposes and the second type built by counting visits to long-live states eliminated noise and was used to show the continuous distribution of long-lived states.

Fluctuating traces, which represent anticorrelated fluctuating FRET signals before photobleaching, were subjected to cross-correlation analysis. The cross-correlation function is defined as previously described (46). Only fluctuation periods >30 s were included in the analysis and the correlation was calculated up to 15 s. Cross-correlation analysis of fluctuations in free NF-κB could be fitted with double exponentials but not with a single exponential (Supplementary Figure S5A and B). Fitting with three exponentials did not significantly reduce the residuals. To examine if there were multiple or even a continuous distribution of time constants underlying the fluctuations, we further analyzed the cross-correlation with the maximum entropy method (MEM) which is well suited to describe a continuous distribution of decay time constants and has been applied to studies of protein folding and ligand binding kinetics by time-resolved spectroscopy to describe system heterogeneity (47). We used Memexp to fit the cross-correlation

iteratively to maximize the Shannon entropy subject to constrained goodness-of-fit (48). Unlike discrete exponential fitting, which requires specification of the number of exponentials, the MEM does not require *a priori* knowledge of the time constant distribution. If there were more than two time constants or a time constant distribution underlying the NF-κB domain fluctuations, we would expect this to be revealed by the MEM fitting.

Molecular simulations and analysis

We used OpenAWSEM (49) to model the DNA/NF-κB complex. The initial structures of the protein and DNA were from the crystal structure of NF-κB (PDB entry: 1LE5). We extended the DNA sequence 100 base pairs of A/T at both ends to reduce any finite size effect caused by having a short DNA sequence. The protein and DNA were initially placed far away from each other. Chain A (RelA) of the protein was shifted 300 Å to the left along the *x*-axis from the DNA and chain B (p50) was shifted 300 Å to the right. As the simulation began, both chains of the protein were pulled toward the DNA with a native protein–DNA contact bias. This bias was turned off after 10 million steps. Then, we ran another 10 million steps of unbiased simulation. We used a Langevin integrator with a friction of 1 ps^{-1} and a step size of 2 fs. The simulations were carried out at constant temperature of 300 K. The default strength for each term followed our previous study (10), with $V_{contact} = 0.75$, $V_{HB} = 0.5$. We did not use a Gō term in this study. The fragment memory consisted of nine equally weighted structures. Among them, one was the crystal structure, and the other 8 structures are sampled from two independent all-atom simulations (31) at 100, 200, 300 and 400 ns. The simulations were repeated 20 times with the same initial structures but different initial velocities and different random seeds. The trajectories were saved every 4000 steps and the last 2000 frames were used for analysis.

RESULTS

smFRET reveals conformational heterogeneity in free NF-κB

Previous coarse-grained (10) and all-atom MD simulations (31) showed that the two NTDs in an NF-κB dimer can rotate and translate with respect to each other. To experimentally probe the conformational heterogeneity of the NTDs, we carried out TIRF-based smFRET experiments by labeling each NTD with either a donor or acceptor fluorophore. We replaced RelA Gln128 and p50 Phe148 with p-azidophenylalanines (pAzF) by amber suppression and then labeled these two residues specifically with either Alexa Fluor 555 or Alexa Fluor 647 sDIBO alkyne via click chemistry (50,51). The distances between the labeling positions in the NF-κB/DNA crystal structure (52) and in an open conformation obtained from previous all-atom simulations (31) are 27 and 70 Å, respectively, corresponding to 0.1 and 1 in FRET efficiency given the 51 Å Förster distance of the dye pair (Figure 2A). The dual-labeled NF-κB was immobilized on a passivated microscope slide (44) through a series of interactions between the C-terminal His-tag on RelA, biotin-conjugated anti-His antibody, NeutrAvidin and biotin conjugated bovine serum albumin (BSA) (Figure 2B). We collected 426 smFRET traces for free NF-κB. Each smFRET trace covers between 10 and 300 s depending on the photobleaching lifetime of the fluorophores. The FRET histogram showed a broad distribution in FRET efficiencies from 0.1 to 1 (Figure 2C), revealing a conformational heterogeneity which corresponds to approximate distances of 30 to 70 Å between the two NTDs in free NF-κB. The distances we report are close estimates based on rigorous background and donor leakage corrections. Obtaining accurate distances from smFRET requires alternating two-color laser excitation (53) and is not the focus of this work.

Free NF-κB adopts a continuum of long-lived conformational states

The smFRET traces showing the time trajectory of single donor and acceptor fluorescence were further classified as stable (82% of the traces) or fluctuating (18% of the traces) (Figure 2C). A stable trace was defined as containing a long-lived FRET state with a lifetime longer than the photobleaching lifetime in that trace (Figure 2E and F), which averaged 90 s (Supplementary Figure S1); a fluctuating trace was characterized by frequent anticorrelation between donor and acceptor signals. Stable traces containing long-lived states with FRET efficiencies from low to high were all observed (Figure 2E). To avoid artificial broadening in the histogram caused by noise, in addition to building the conventional FRET histogram by binning 0.1 s time windows (Figure 2C), we constructed a histogram for long-lived states by binning the mean FRET efficiency of each visit to a state (Figure 2D). The histogram constructed in this way showed that these long-lived states could not be separated into discrete groups. Instead, we observed a heterogeneous, continuous distribution between high and low FRET efficiencies. In 13 of the traces, we observed transitions between a few long-lived states (Figure 2F and Supplementary Figure S2A), suggesting that the long-lived states can interconvert via slow dynamics likely on the minutes timescale. A continuum of long-lived states and transitions between them were still observed in the presence of DTT (1 mM), indicating that the heterogeneity was not caused by the formation of disulfide bonds (Supplementary Figure S3).

DNA-bound NF-κB adopts a distribution of long-lived conformational states including partially bound states

We next investigated the conformational heterogeneity in DNA-bound NF-κB by carrying out smFRET experiments with dual-labeled NF-κB bound to a biotinylated hairpin DNA containing a κB binding site which was immobilized on a passivated surface through biotin–NeutrAvidin interactions (Figure 3A). By immobilizing through biotinylated DNA, we ensured that every NF-κB molecule observed was bound to DNA. We collected 199 smFRET traces for DNA-bound NF-κB, of which 84% could be classified as stable—containing a long-lived state with a lifetime longer than the photobleaching lifetime (Supplementary Figure S1). Surprisingly, DNA did not shift the conformational

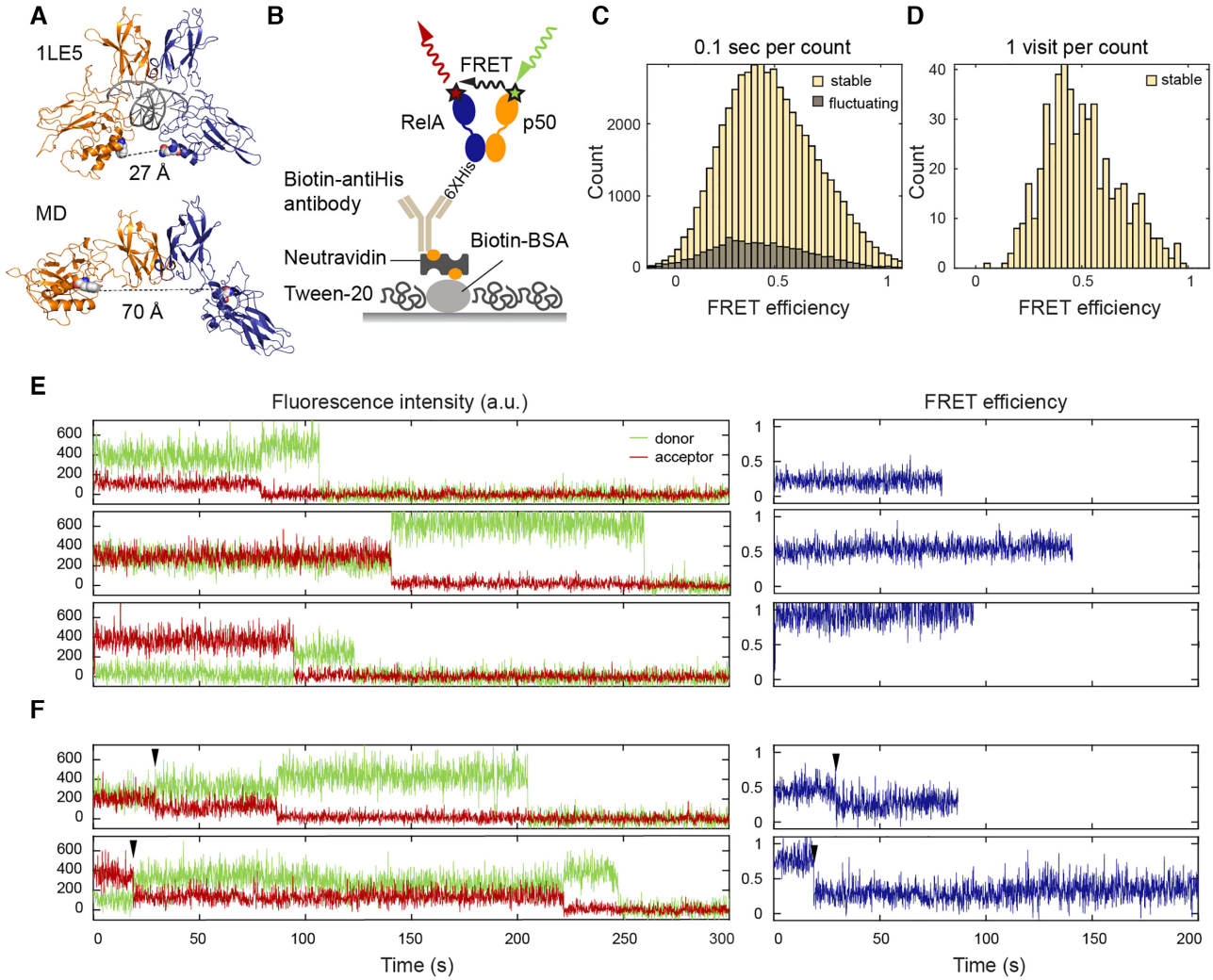

Figure 2. smFRET revealed a continuum of long-lived conformations for free NF-κB. (**A**) In the NF-κB/DNA structure (PDB: 1LE5), the distance between the labeled positions (spheres) would lead to a high FRET efficiency ∼1. In MD simulations, free NF-κB could adopt an open conformation, leading to a low FRET efficiency ∼0.1. (**B**) Schematic of NF-κB immobilization on a DT20 passivated surface. (**C**) FRET histogram showing a broad distribution of conformations. The histogram was constructed by counting every 0.1 s time window in the first 10 s of all traces. (**D**) FRET histogram constructed by counting each visit to a long-lived state suggested a continuum that cannot be separated into a few groups. (**E**) Representative long-lived states with low, mid and high FRET efficiencies. Sudden drops of the donor or acceptor signals to zero indicate single photobleaching events. (**F**) Transitions (arrowhead) between long-lived states were captured in a subset of traces.

ensemble to a single high-FRET state as expected from the crystal structure but instead shifted the distribution of long-lived states to two major populations including a high-FRET population in good agreement with the structure, as well as an unexpected low-FRET population (Figure 3B and C). Despite these two dominating populations, a continuum of long-lived states including those with mid-FRET efficiencies was observed (Figure 3E). As was the case for free NF-κB, transitions between long-lived states were captured in five traces (Figure 3F and Supplementary Figure S2B), suggesting interdomain motions on the minutes timescale. Since all crystal structures of DNA-bound NF-κB indicate a ∼30 Å distance between the labeling positions (PDB entries: 1VKX, 1LE5, 1LE9, 1LEI, 2I9T, 2O61 and 3GUT), we were surprised to observe a major population of DNA-bound NF-κB at low FRET efficiency. A crystal structure of NF-κB p50 homodimer bound to two double-stranded RNA molecules (54) suggested such a low-FRET state could be caused by binding to two copies of DNA on the microscope slide, forcing the NTDs to spread apart. To test this possibility, we carried out smFRET titration experiments, this time immobilizing NF-κB and varying DNA concentrations in the solution (Figure 3G). If the low-FRET state was a conformation caused by binding to two DNA molecules, the relative peak height for the low-FRET population would increase as the DNA concentration increased. Because the NF-κB is immobilized, we expect a population of free NF-κB to also contribute to the histogram. The results showed that a range of NF-κB:DNA molar ratios from 10:1 to 1:100 lead to almost identical FRET histograms. Each histogram appears to have two slightly higher peaks at high and low FRET efficiencies

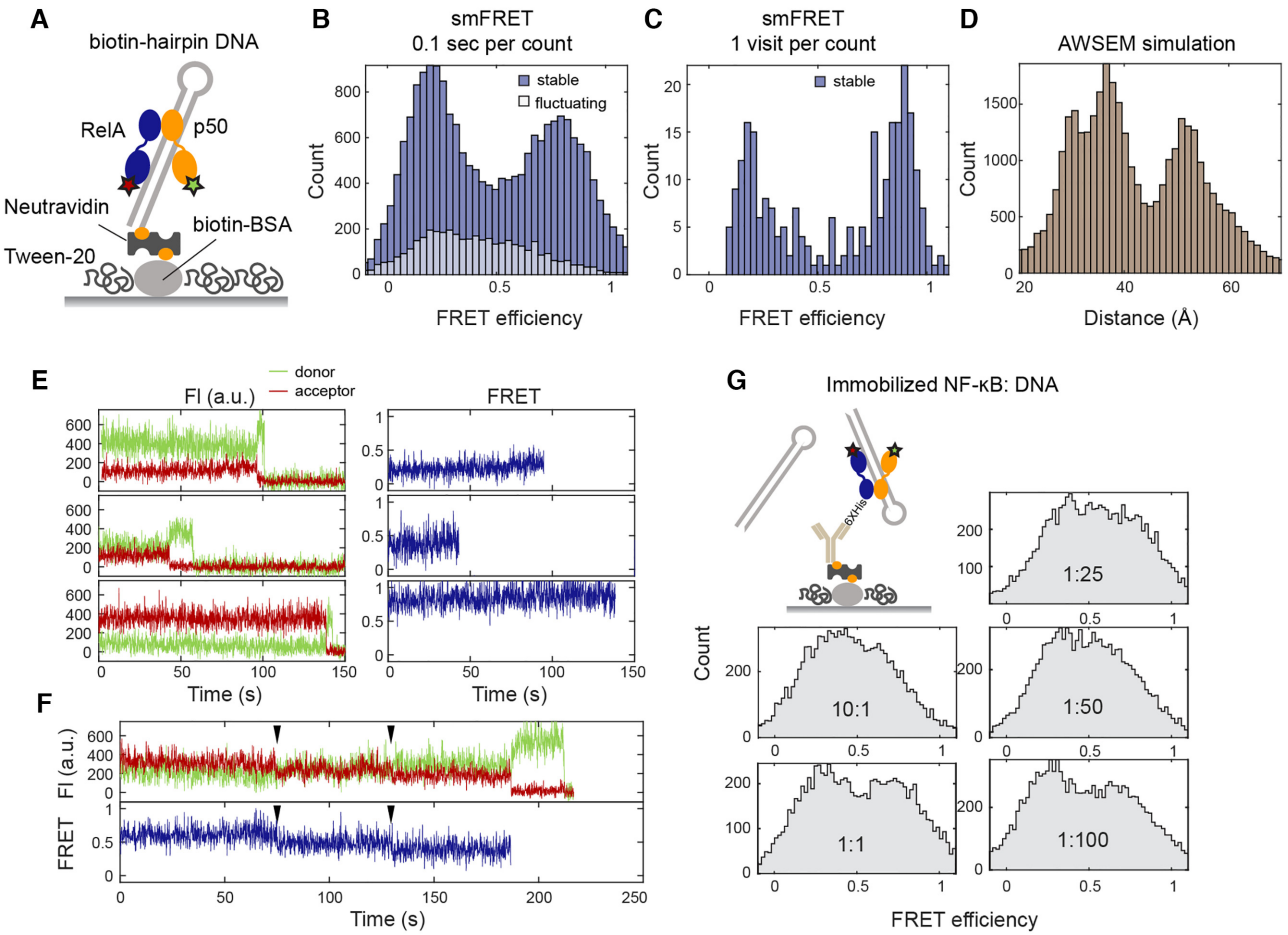

Figure 3. smFRET revealed a continuum of long-lived conformations for DNA-bound NF-κB. (**A**) A biotinylated hairpin DNA with a κB site was used for immobilization through biotin–NeutrAvidin interactions. (**B**) FRET histogram showing two major populations at low and high FRET efficiencies contributed by stable traces. (**C**) FRET histogram constructed by counting each visit to a long-lived state showing a continuous distribution with two dominating populations. (**D**) Distance distribution of between labeling positions by AWSEM simulations showing two dominating populations in DNA-bound NF-κB. (**E**) Representative stable traces showing long-lived states with low, mid, and high FRET efficiencies for DNA-bound NF-κB. (**F**) A representative trace showing transitions between long-lived states from high to mid to low FRET efficiencies. (**G**) smFRET titration experiments with immobilized NF-κB and varying DNA concentrations. A series of NF-κB:DNA molar ratios from 10:1 to 1:100 showed similar FRET histograms with a broad band from free NF-κB and two slightly higher peaks at low and high FRET efficiencies from DNA-bound NF-κB.

contributed by DNA-bound NF-κB superimposed on the broad distribution from free NF-κB (Figure 3G). The independence of the FRET histogram on the DNA concentration suggests that the low-FRET state was not a conformation resulting from binding to two copies of DNA but is likely a conformation with one NTD dissociated from DNA.

To understand whether the low FRET population could be due to NF-κB bound to one copy of DNA, we performed coarse-grained AWSEM simulations (10,49). Indeed, constant temperature simulations revealed a similar broad distribution in distances between labeling positions with a major population of ∼30 Å distance as in the crystal structure and another major population with a larger distance that would lead to lower FRET (Figure 3D). Together, the results suggest that within the broad conformational distribution of DNA-bound NF-κB, there are two major populations corresponding to a fully bound state (high FRET) and a partially bound state with the NTDs too far apart to both engage the DNA (low FRET) respectively.

Free and DNA-bound NF-κB undergo interdomain motions on the seconds timescale

Besides the stable traces observed for free NF-κB, anticorrelated fluctuating FRET signals were observed in 18% of the smFRET traces (Figure 2C). In some traces, the motions were large enough to connect low- and high-FRET states, corresponding to a 70 to 30 Å interdomain distance change (Figure 4A). The motions displayed a high level of heterogeneity and, as was the case for the long-lived states, could not be described by a few discrete groups. In other traces (Figure 4B), the two domains fluctuated around ∼0.25 FRET efficiency (distance ∼60 Å), and then transitioned to a state with ∼0.8 FRET efficiency (distance ∼40 Å) and fluctuated around that value, showing the hierarchical organization of the energy landscape. We also observed that NF-κB molecules transitioned from a fluctuating state to a long-lived state where they could be temporarily trapped (Figure 4C). Such transitions between states with fluctuating FRET and long-lived states were captured

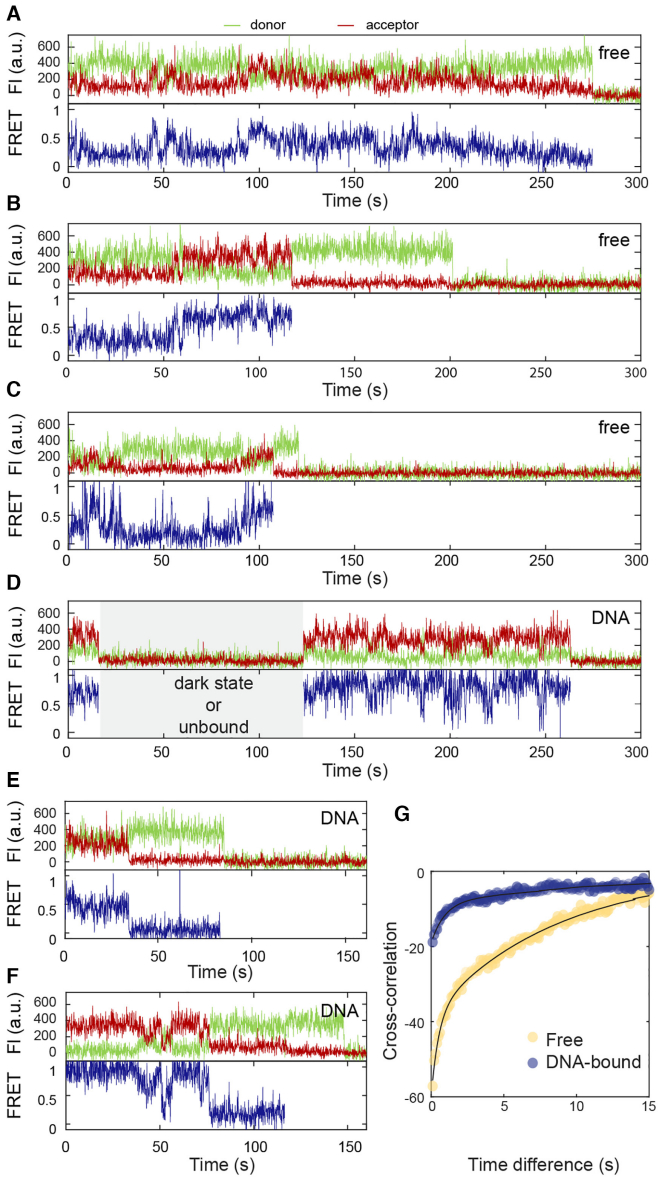

Figure 4. Interdomain motions of free and DNA-bound NF-κB on the seconds timescale. (**A**) A representative fluctuating trace for free NF-κB with fluctuations connecting low- and high- FRET states, which corresponds 30–70 Å in the interdomain distance. (**B**) A trace for free NF-κB with small fluctuations around a low-FRET state at first. At 60 s, the molecule transitioned to a high-FRET state and fluctuated around it. (**C**) A trace with transitions between fluctuations and long-lived states for free NF-κB, suggesting all the conformational states are interconvertible. (**D** and **E**) Representative fluctuating traces of DNA-bound NF-κB showing small fluctuations. The time period with no signals (gray area) could be caused by a donor dark state, an unbound state, or a state in which an unlabeled NF-κB is bound to the immobilized DNA, and does not affect data interpretation. (**F**) A trace with transitions between fluctuating and long-lived states for DNA-bound NF-κB. (**G**) Cross-correlation analyses for fluctuations of free (yellow) and DNA-bound (blue) NF-κB showing that the interdomain motions of the DNA-bound NF-κB have lower amplitudes and slower rates. Biexponential fitting revealed the characteristic fluctuation time to be 0.50 ± 0.08 s and 8.4 ± 0.7 s for free NF-κB and 0.91 ± 0.16 s and 17 ± 3 s for DNA-bound NF-κB.

in 26 traces (6.1% of all the traces) (Supplementary Figure S4). This again confirmed that the long-lived states are not static but are interconvertible with one another and with other shorter-lived conformational states.

The fluctuations were subjected to cross-correlation analysis for the donor and acceptor signals. The cross-correlation monotonically decayed as a function of time, suggesting no periodicity for the interdomain motions and reflecting the stochastic diffusion-like dynamics of single protein domains (Figure 4G). The cross-correlation for fluctuations in free NF-κB is best described by a biexponential function giving decay time constants 0.50 ± 0.08 s and 8.4 ± 0.7 s with corresponding amplitudes −22 ± 2 and −38 ± 1 respectively (Supplementary Figure S5). Fitting with the MEM gave two narrow populations of decay time constants of 0.4 ± 0.1 and 2.2 ± 0.7 s, instead of a broad distribution (Supplementary Figure S5C and D). It is known that the MEM analysis can give consistent shapes of time constant distributions, but the errors in the values of time constants were larger than those from exponential fitting (55). Importantly, the MEM reveals two narrow populations rather than a broad distribution. The consistency of the results from both MEM and exponential fitting gives us confidence that the domain fluctuations of NF-κB are best described by the two characteristic time constants from biexponential fitting.

We also examined the effect of ionic strength on the interdomain motions. A series of smFRET experiments with NaCl concentrations from 100 to 250 mM showed that the percentage of fluctuating traces (Supplementary Figure S6A) and fluctuating time scale (Supplementary Figure S6B) are dependent on ionic strength but not with a simple monotonic trend.

NF-κB bound to immobilized DNA also showed fluctuations on the seconds timescale. However, large-scale fluctuations connecting 70 and 30 Å interdomain distances were no longer observed (Figure 4D and E). Cross-correlation analysis of fluctuations in DNA-bound NF-κB yielded decay time constants of 0.91 ± 0.16 s and 17 ± 3 s with amplitudes of −11 ± 1 and −8.4 ± 0.6, respectively (Figure 4G). The smaller amplitudes compared to those in free NF-κB reflect the lack of large-scale fluctuations. Both times are two-fold slower than those for free NF-κB. Fitting of the DNA-bound data with MEM also showed two narrow populations of the decay time constants of 1.4 ± 0.4 and 13.4 ± 2.3. s. The larger values for the time constants for DNA-bound NF-κB compared to those for free NF-κB (Supplementary Figure S5D), are consistent with exponential fitting. We expect that the decreased fluctuation amplitudes and rates for DNA-bound NF-κB are results of the additional electrostatic interactions introduced by the negatively charged DNA. As in free NF-κB, 3.0% of DNA-bound NF-κB molecules also transitioned between fluctuating states and long-lived states (Figure 4F and Supplementary Figure S7).

For both free and DNA-bound NFκB molecules, the two time constants derived from the cross-correlation analysis are only part of the story. Given the diversity of FRET values represented in the fluctuating traces, it was likely there were more than two kinds of reconfiguration processes that underlaid the fluctuations. In addition, the cross-

correlation analysis did not capture transitions to and from the long-lived stable FRET states. There were 12 traces in which free NF-κB molecules showed a long-lived state preceded and followed by periods of fluctuating FRET. From these, we could obtain an average dwell time in the stable state of 36 ± 17 s. A similarly wide distribution of dwell times (from 4 to 96 s) was observed for molecules in a period of fluctuating FRET that was preceded and followed by a long-lived FRET state (Supplementary Figure S4). We conclude that the energy landscape is rugged with deep energy wells corresponding to the heterogeneous long-lived states superimposed on states separated by smaller barriers with two kinds of heights. These barriers may locate within each of the deep wells, as suggested by fast fluctuations around different FRET values displayed in individual traces.

IκBα binding eliminates NF-κB conformational heterogeneity

To investigate how the inhibitor protein, IκBα, that strips NF-κB from DNA and inhibits DNA binding affects the interdomain motions of NF-κB, we carried out smFRET experiments with dual-labeled non-tagged NF-κB bound to immobilized IκBα (Figure 5A). By immobilizing through His-tagged IκBα, we ensured that every NF-κB molecule observed is bound to IκBα. The FRET histogram and traces showed that every IκBα-bound NF-κB molecule populated a stable low-FRET state (Figure 5B and E). The histogram built by counting each visit to a long-lived state revealed a narrow conformational distribution in the range of 0.1 to 0.4 FRET efficiency (56 to 74 Å in distance) (Supplementary Figure S8). All traces contained long-lived states with lifetime longer than the photobleaching lifetime. No anticorrelated donor and acceptor signals were observed (Supplementary Figure S9), suggesting the interdomain motions displayed in free and DNA-bound NF-κB were completely suppressed by IκBα. Transitions between long-lived states were not observed either. The results show that IκBα eliminated the conformational heterogeneity in NF-κB and locked the interdomain motions in a static state consistent with NTDs being spread apart.

We next performed the same experiment for NF-κB bound to the 5xPEST IκBα mutant, which contains charge-neutralizing mutations E282Q/E284Q/D285N/E286Q/E287Q in the C-terminal disordered PEST sequence and is not able to strip NF-κB or completely inhibit DNA binding (27) (Figure 5C). The results showed that, in contrast to wild-type, 5xPEST IκBα was not able to lock the NF-κB interdomain motions in a static state. Instead, 5xPEST IκBα-bound NF-κB displayed a continuum of states and domain fluctuations as was observed for free NF-κB (Figure 5D and F). Interestingly, we observed a higher proportion of fluctuating traces in 5xPEST IκBα-bound NF-κB (35%) as compared in free NF-κB (17%), implying that placing a charge-neutral polypeptide in between the NF-κB NTDs disrupts interactions that lead to long-lived states. Our results show that the DNA binding function of NF-κB is associated with its interdomain motions and that the stripping and inhibitory function of IκBα is related to its ability to lock the NF-κB NTDs in a fixed position.

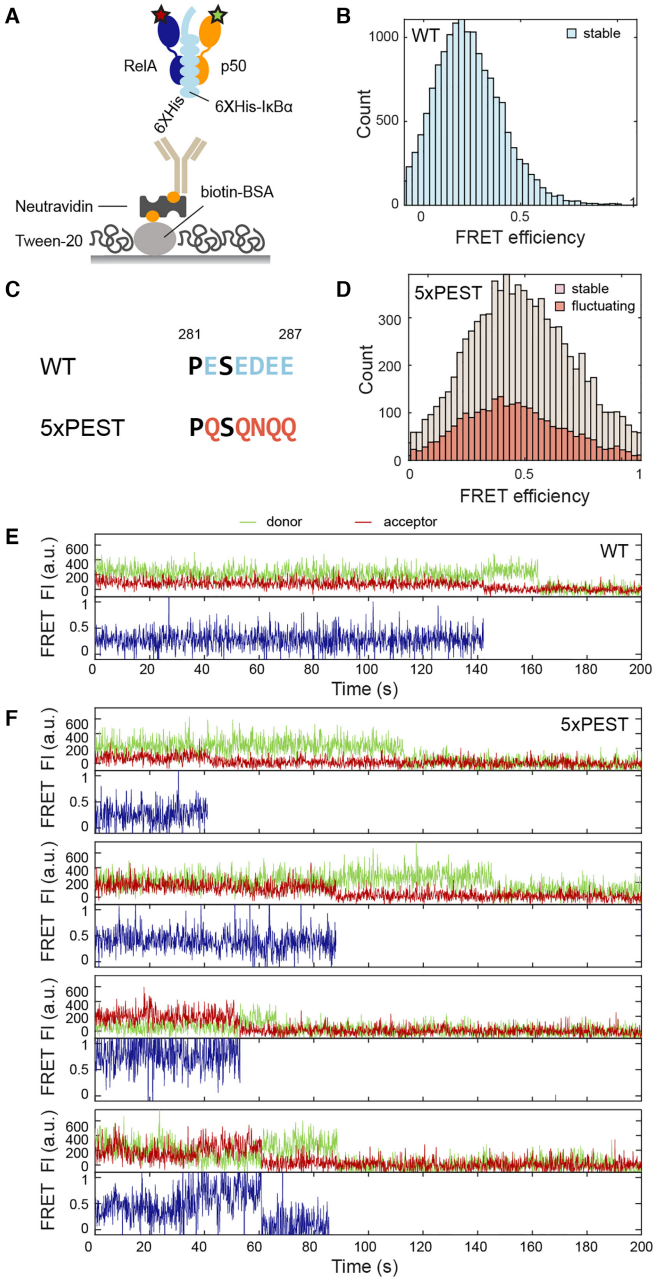

Figure 5. Elimination of conformational heterogeneity of NF-κB by IκBα but not by the 5xPEST IκBα. (**A**) The His-tag on IκBα was used to immobilize the NF-κB through the interaction with anti-His antibody biotin conjugate. (**B**) FRET histogram of NF-κB bound to wildtype (WT) IκBα showing only a stable low FRET state was observed. (**C**) The stripping impaired 5xPEST IκBα mutant contains five mutations in the PEST sequence to neutralize negatively charged residues. (**D**) FRET histogram for NF-κB bound to the 5xPEST IκBα showing a broad distribution and a larger proportion of fluctuating traces. (**E**) A representative trace of NF-κB bound to WT IκBα showing the stable low-FRET state. (**F**) Representative traces of NF-κB bound to 5xPEST IκBα showing heterogeneous long-lived states with a range of FRET efficiencies and domain fluctuations.

DISCUSSION

Gene regulation is under kinetic control (3,5,10–12), in which binding and unbinding of transcription factors to DNA regulate the transcriptional outcome (9,15,16). To

gain a molecular picture of how the on and off rates of transcription factor binding to DNA are controlled, we directly visualized the conformational states of NF-κB and the dynamics of their interconversion at the single-molecule level with TIRF-based smFRET. Our results revealed a remarkable continuum of conformations for NF-κB in the free and DNA-bound states, connected by motions on a range of timescales from hundreds of milliseconds to minutes (Figure 6). The majority of the molecules, either free or DNA-bound, were found to reside in long-lived states interconverting on the minutes timescale, slower than the average *in vivo* dwell time of NF-κB on DNA, which is 4.1 s by single-molecule tracking (30). Compared to the dwell time of seconds measured *in vivo*, the minute-long conformations of DNA-bound NF-κB would appear static during its residence on DNA, and each of the diverse bound conformations would likely lead to a unique off rate, consistent with the continuous distribution of rates observed in live cells (15,16).

Similarly, the continuum of conformations in free NF-κB would lead to a distribution of on rates. The average on rate (k_{on}×[DNA]) of NF-κB from single-molecule tracking experiments is 6.7×10^{-2} s^{-1} (30), translating to a binding event for an NF-κB molecule every 15 s. Again, the long-lived conformations of free NF-κB would appear static from the viewpoint of DNA binding. In previous bulk experiments, we showed that the on rates of NF-κB dimers correlate with the degree of DNA-binding cavity exposure (31). The broad distribution of conformations of the NF-κB RelA-p50 heterodimer we resolve with smFRET, each with different DNA accessibility, would result in a continuum of on rates. We also observed more rapid opening and closing of the DNA-binding cavity with fluctuations on the seconds timescale for free NF-κB, which might allow for rapid DNA engagement by both domains in the time frame of a single binding event (15 s).

Our observation of a continuum of conformations sheds light on the mechanism of molecular stripping (10), a dissociation mechanism in which the off rate is enhanced by a competitor protein forming a transient ternary complex to lower the dissociation barrier (10,26,27,56). Here we showed that much of the DNA-bound NF-κB does not have both NTDs bound to the DNA, leaving the DNA-binding cavity vulnerable to invasion by IκBα. Binding of IκBα eliminated interdomain motions, rigidifying NF-κB into a static state with the NTDs too far apart to both engage DNA. Whereas the 5xPEST IκBα mutant, which is unable to strip NF-κB or completely inhibit DNA binding (27), was unable to elicit the static structure. Our results suggest that the conformational flexibility of NF-κB is required for DNA binding, and that molecular stripping is a process of eliminating such flexibility by IκBα to facilitate the release of DNA and prevent DNA rebinding.

Both conformational flexibility and multivalent interactions together allow facilitated dissociation either by the same protein (18,20,21,23) or by a different inhibitor (25,28,29). These two features enable the visitation of partially bound states and responses to the competitor proteins. Indeed, all the DNA-binding proteins that undergo self-facilitated dissociation are dimers or multidomain proteins with interdomain flexibility and multivalent interactions with DNA (18,20,21,23). Likewise, several proteins that undergo inhibitor-facilitated dissociation such as TAZ1/CITED2 and histone H1/prothymosin α are intrinsically disordered with multivalency (28,29). In the case of NF-κB, a continuum of bound states connected by slow interdomain motions allows IκBα to invade the partially exposed DNA-binding cavity and accelerate DNA dissoci-

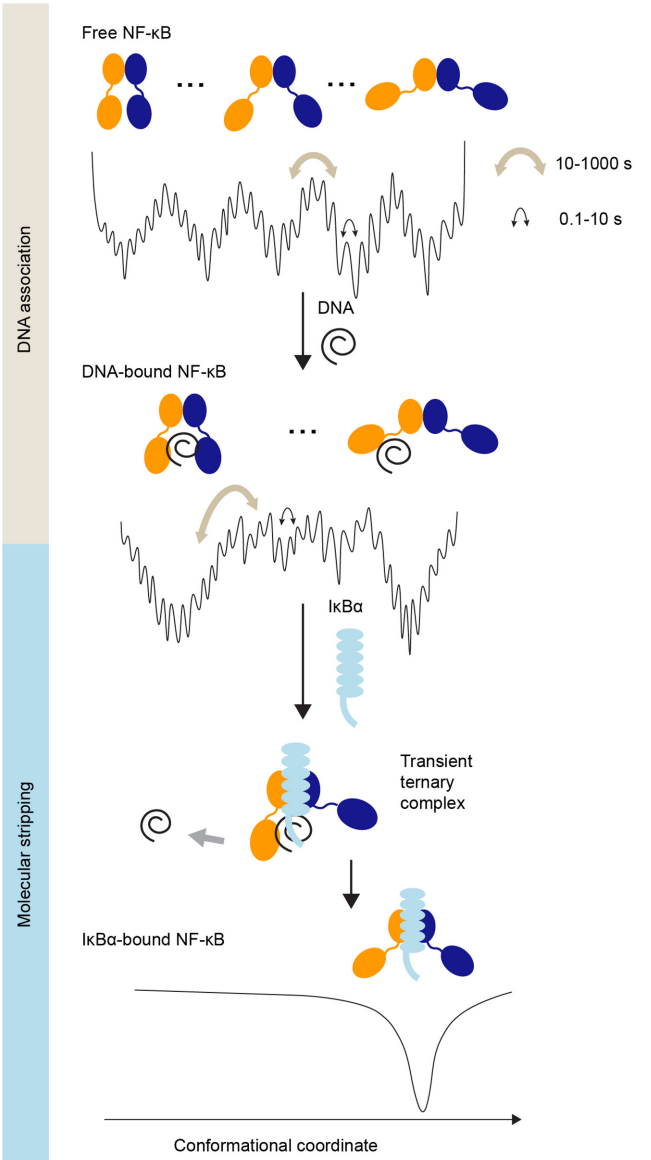

Figure 6. NF-κB utilizes a continuum of binding modes for DNA association and molecular stripping. The energy landscape of free NF-κB is highly rugged and hierarchically organized, resulting in a continuum of conformations interconverting on the subseconds to minutes timescale, comparable to *in vivo* binding on the seconds timescale. Free NF-κB adopts a broad distribution of conformations, each with a different degree of DNA accessibility. DNA-bound NF-κB also adopts a continuum of distributions, which leads to a continuum of off rates in cells. The two major populations of DNA-bound NF-κB correspond to a fully bound state and a partially bound state; the latter allows the invasion of IκBα to form a ternary complex and eventually strip NF-κB from DNA. Binding of IκBα facilitates DNA dissociation and inhibits DNA binding by inducing a single static conformation in NF-κB where the NTDs are too far apart to both engage DNA.

ation. Since nearly all transcription factors are dimers and contain IDRs (57,58), it is likely that many more will display similar continua of conformations and binding rates for exquisite kinetic control.

Our results provide a first glimpse of a resolved and visualized continuum of conformations connected by extremely slow motions. Historically, navigation through a protein energy landscape has been depicted as interconversion between a few discrete, low-energy states (59). Surprisingly, our results reveal a hierarchical rugged energy landscape with many deep wells leading to a continuum of long-lived conformational states interconvertible on the minutes timescale superimposed on a rough surface of substates that interconvert on the hundreds of milliseconds to seconds timescale (Figure 6). Similar findings of multiple continuous conformations and sub-diffusive dynamics on a rugged energy landscape have been reported by kinetic analyses of single-molecule experiments and NMR experiments (60–63). Yet this is the first time that such slow and heterogeneous motions are visualized in real time. Two features of the NF-κB molecule may be responsible for such slow motions. First, the ionic strength dependence of the slow NF-κB motions suggests they originate from balancing attractive and repulsive interactions from the non-uniform charge distribution. The frustration between the many possible electrostatic interactions would lead to a highly rugged energy landscape with a broad distribution of long-lived conformational states. Indeed, the addition of the negatively charged DNA caused the interdomain motions to be even slower and of reduced amplitude, while the addition of the 5xPEST IκBα mutant with a charge-neutral PEST sequence results in an increased fraction of fluctuating traces. The comparison between wildtype and 5xPEST IκBα also suggests that elimination of the conformational flexibility is achieved through the negatively charged PEST sequence. Second, the highly conserved linker of NF-κB, with the sequence DNRAPNTAEL for RelA and DSKAPNASNL for p50, contains a proline and several charged residues, both of which are known to affect the rigidity and compactness of disordered linkers (64) and may lead to slow interdomain motions. In addition, prolines in the linkers can undergo *cis–trans* isomerization on seconds to minutes timescale (65) and therefore could also contribute to the slow motions.

It is never simple to relate *in vitro* observations to *in vivo* phenomena. What would our finding of a continuum of slowly interconverting conformations for NF-κB imply in the cellular context? In our experiments, only short DNA fragments with single κB sites were used, thus not directly reflecting the crowded yet highly organized nuclear environment. Besides transcription factors, there are also many other players in transcriptional regulation including chromatin remodelers, transcription coactivators, enhancers, etc. All these additional components can lead to phenomena unexpected from isolated transcription factors on the smFRET microscope slide. In a complex environment like the cell, however, molecular behaviors of individual proteins are hidden. The purpose of *in vitro* single-molecule experiments is to resolve those molecular behaviors critical to function by eliminating confounding variables. Indeed, even when bound to a simplified DNA molecule, NF-κB displays profound conformational heterogeneity and responds to wild-type versus mutant IκBα differently. Such molecular behaviors, which are not accessible by *in vivo* approaches, explain the broad distribution of off rates of transcription factors as well as how IκBα is able to terminate the NF-κB response efficiently *in vivo* while the 5xPEST IκBα mutant is not (27). To further test our proposed mechanism of controlling the on and off rates of NF-κB by conformational dynamics, it will be necessary to identify mutations or other inhibitors that perturb the interdomain motions to further examine their effects on *in vivo* binding kinetics and transcriptional outcomes in the cellular context. However, given the complexity of the molecular motions we observe, it seems unlikely that the effect of individual mutations will be simple to interpret.

In conclusion, our direct visualization of the single-molecule conformational dynamics of the transcription factor NF-κB reveals a continuum of binding modes for DNA association and IκBα facilitated dissociation known as molecular stripping. Our results suggest a novel binding mechanism for kinetically controlling the on rate and off rate of transcription factor binding to DNA. Despite our focus on transcription, this binding mechanism may be prevalent in other aspects of cellular functions where a kinetic control of both association and dissociation is needed.

DATA AVAILABILITY

Single-molecule FRET traces are available on https://github.com/komiveslab/NFkB_smFRET_traces.

SUPPLEMENTARY DATA

Supplementary Data are available at NAR Online.

ACKNOWLEDGEMENTS

We thank Hajin Kim at Ulsan National Institute of Science and Technology for his advice on setting up the TIRF microscope, Majid Ghassemian at the Biomolecular and Proteomics Mass Spectrometry Facility of UCSD for carrying out the mass spectrometry analyses, Hannah Baughman for critically reading the manuscript and providing constructive feedback, and Andy McCammon for helpful discussions. W.C. thanks Chi-Yun Lin for helpful discussions.

Author Contributions: W.C. designed and performed experiments, analyzed data and wrote the manuscript. W.L. performed and analyzed simulations. P.G.W. supervised simulations. E.A.K. designed experiments and wrote the manuscript.

FUNDING

NIH [P01GM071862]; Mathers Foundation [MF-2012-01149]; Ministry of Education of Taiwan [1061110016 to W.C.]. Funding for open access charge: Mathers Foundation [MF-2012-01149].

Conflict of interest statement. None declared.

REFERENCES

1. Lambert,S.A., Jolma,A., Campitelli,L.F., Das,P.K., Yin,Y., Albu,M., Chen,X., Taipale,J., Hughes,T.R. and Weirauch,M.T. (2018) The human transcription factors. *Cell*, **172**, 650–665.
2. Larson,D.R., Fritzsch,C., Sun,L., Meng,X., Lawrence,D.S. and Singer,R.H. (2013) Direct observation of frequency modulated transcription in single cells using light activation. *Elife*, **2**, e00750.
3. Zoller,B., Little,S.C. and Gregor,T. (2018) Diverse spatial expression patterns emerge from unified kinetics of transcriptional bursting. *Cell*, **175**, 835–847.
4. Fukaya,T., Lim,B. and Levine,M. (2016) Enhancer control of transcriptional bursting. *Cell*, **166**, 358–368.
5. Li,C., Cesbron,F., Oehler,M., Brunner,M. and Hofer,T. (2018) Frequency modulation of transcriptional bursting enables sensitive and rapid gene regulation. *Cell Syst.*, **6**, 409–423.
6. Lammers,N.C., Galstyan,V., Reimer,A., Medin,S.A., Wiggins,C.H. and Garcia,H.G. (2020) Multimodal transcriptional control of pattern formation in embryonic development. *Proc. Natl. Acad. Sci. U.S.A.*, **117**, 836–847.
7. Stavreva,D.A., Garcia,D.A., Fettweis,G., Gudla,P.R., Zaki,G.F., Soni,V., McGowan,A., Williams,G., Huynh,A., Palangat,M. *et al.* (2019) Transcriptional bursting and co-bursting regulation by steroid hormone release pattern and transcription factor mobility. *Mol. Cell*, **75**, 1161–1177.
8. Donovan,B.T., Huynh,A., Ball,D.A., Patel,H.P., Poirier,M.G., Larson,D.R., Ferguson,M.L. and Lenstra,T.L. (2019) Live-cell imaging reveals the interplay between transcription factors, nucleosomes, and bursting. *EMBO J.*, **38**, e100809.
9. Mueller,F., Stasevich,T.J., Mazza,D. and McNally,J.G. (2013) Quantifying transcription factor kinetics: at work or at play? *Crit. Rev. Biochem. Mol. Biol.*, **48**, 492–514.
10. Potoyan,D.A., Zheng,W., Komives,E.A. and Wolynes,P.G. (2016) Molecular stripping in the NF-kappaB/IkappaB/DNA genetic regulatory network. *Proc. Natl. Acad. Sci. U.S.A.*, **113**, 110–115.
11. Scholes,C., DePace,A.H. and Sanchez,A. (2017) Combinatorial gene regulation through kinetic control of the transcription cycle. *Cell Syst.*, **4**, 97–108.
12. Wong,F. and Gunawardena,J. (2020) Gene regulation in and out of equilibrium. *Annu. Rev. Biophys.*, **49**, 199–226.
13. Bintu,L., Buchler,N.E., Garcia,H.G., Gerland,U., Hwa,T., Kondev,J. and Phillips,R. (2005) Transcriptional regulation by the numbers: models. *Curr. Opin. Genet. Dev.*, **15**, 116–124.
14. Segal,E., Raveh-Sadka,T., Schroeder,M., Unnerstall,U. and Gaul,U. (2008) Predicting expression patterns from regulatory sequence in Drosophila segmentation. *Nature*, **451**, 535–540.
15. Garcia,D.A., Fettweis,G., Presman,D.M., Paakinaho,V., Jarzynski,C., Upadhyaya,A. and Hager,G.L. (2021) Power-law behavior of transcription factor dynamics at the single-molecule level implies a continuum affinity model. *Nucleic Acids Res.*, **49**, 6605–6620.
16. Garcia,D.A., Johnson,T.A., Presman,D.M., Fettweis,G., Wagh,K., Rinaldi,L., Stavreva,D.A., Paakinaho,V., Jensen,R.A.M., Mandrup,S. *et al.* (2021) An intrinsically disordered region-mediated confinement state contributes to the dynamics and function of transcription factors. *Mol. Cell*, **81**, 1484–1498.
17. Morisaki,T., Muller,W.G., Golob,N., Mazza,D. and McNally,J.G. (2014) Single-molecule analysis of transcription factor binding at transcription sites in live cells. *Nat. Commun.*, **5**, 4456.
18. Graham,J.S., Johnson,R.C. and Marko,J.F. (2011) Concentration-dependent exchange accelerates turnover of proteins bound to double-stranded DNA. *Nucleic Acids Res.*, **39**, 2249–2259.
19. Loparo,J.J., Kulczyk,A.W., Richardson,C.C. and van Oijen,A.M. (2011) Simultaneous single-molecule measurements of phage T7 replisome composition and function reveal the mechanism of polymerase exchange. *Proc. Natl. Acad. Sci. U.S.A.*, **108**, 3584–3589.
20. Joshi,C.P., Panda,D., Martell,D.J., Andoy,N.M., Chen,T.Y., Gaballa,A., Helmann,J.D. and Chen,P. (2012) Direct substitution and assisted dissociation pathways for turning off transcription by a MerR-family metalloregulator. *Proc. Natl. Acad. Sci. U.S.A.*, **109**, 15121–15126.
21. Gibb,B., Ye,L.F., Gergoudis,S.C., Kwon,Y., Niu,H., Sung,P. and Greene,E.C. (2014) Concentration-dependent exchange of replication protein A on single-stranded DNA revealed by single-molecule imaging. *PLoS One*, **9**, e87922.
22. Lewis,J.S., Spenkelink,L.M., Jergic,S., Wood,E.A., Monachino,E., Horan,N.P., Duderstadt,K.E., Cox,M.M., Robinson,A., Dixon,N.E. *et al.* (2017) Single-molecule visualization of fast polymerase turnover in the bacterial replisome. *Elife*, **6**, e23932.
23. Sottini,A., Borgia,A., Borgia,M.B., Bugge,K., Nettels,D., Chowdhury,A., Heidarsson,P.O., Zosel,F., Best,R.B., Kragelund,B.B. *et al.* (2020) Polyelectrolyte interactions enable rapid association and dissociation in high-affinity disordered protein complexes. *Nat. Commun.*, **11**, 5736.
24. Kamar,R.I., Banigan,E.J., Erbas,A., Giuntoli,R.D., Olvera de la Cruz,M., Johnson,R.C. and Marko,J.F. (2017) Facilitated dissociation of transcription factors from single DNA binding sites. *Proc. Natl. Acad. Sci. U.S.A.*, **114**, E3251–E3257.
25. Bergqvist,S., Alverdi,V., Mengel,B., Hoffmann,A., Ghosh,G. and Komives,E.A. (2009) Kinetic enhancement of NF-kappaBxDNA dissociation by IkappaBalpha. *Proc. Natl. Acad. Sci. U.S.A.*, **106**, 19328–19333.
26. Alverdi,V., Hetrick,B., Joseph,S. and Komives,E.A. (2014) Direct observation of a transient ternary complex during IkappaBalpha-mediated dissociation of NF-kappaB from DNA. *Proc. Natl. Acad. Sci. U.S.A.*, **111**, 225–230.
27. Dembinski,H.E., Wismer,K., Vargas,J.D., Suryawanshi,G.W., Kern,N., Kroon,G., Dyson,H.J., Hoffmann,A. and Komives,E.A. (2017) Functional importance of stripping in NFkappaB signaling revealed by a stripping-impaired IkappaBalpha mutant. *Proc. Natl. Acad. Sci. U.S.A.*, **114**, 1916–1921.
28. Heidarsson,P.O., Mercadante,D., Sottini,A., Nettels,D., Borgia,M.B., Borgia,A., Kilic,S., Fierz,B., Best,R.B. and Schuler,B. (2020) Disordered proteins enable histone chaperoning on the nucleosome. bioRxiv doi: https://doi.org/10.1101/2020.04.17.046243, 18 April 2020, preprint: not peer reviewed.
29. Berlow,R.B., Dyson,H.J. and Wright,P.E. (2017) Hypersensitive termination of the hypoxic response by a disordered protein switch. *Nature*, **543**, 447–451.
30. Callegari,A., Sieben,C., Benke,A., Suter,D.M., Fierz,B., Mazza,D. and Manley,S. (2019) Single-molecule dynamics and genome-wide transcriptomics reveal that NF-kB (p65)-DNA binding times can be decoupled from transcriptional activation. *PLos Genet.*, **15**, e1007891.
31. Narang,D., Chen,W., Ricci,C.G. and Komives,E.A. (2018) RelA-containing NFkappaB dimers have strikingly different DNA-binding cavities in the absence of DNA. *J. Mol. Biol.*, **430**, 1510–1520.
32. Baeuerle,P.A. and Baltimore,D. (1988) I kappa B: a specific inhibitor of the NF-kappa B transcription factor. *Science*, **242**, 540–546.
33. Huang,T.T., Kudo,N., Yoshida,M. and Miyamoto,S. (2000) A nuclear export signal in the N-terminal regulatory domain of IkappaBalpha controls cytoplasmic localization of inactive NF-kappaB/IkappaBalpha complexes. *Proc. Natl. Acad. Sci. U.S.A.*, **97**, 1014–1019.
34. Johnson,C., Van Antwerp,D. and Hope,T.J. (1999) An N-terminal nuclear export signal is required for the nucleocytoplasmic shuttling of IkappaBalpha. *EMBO J.*, **18**, 6682–6693.
35. Birbach,A., Gold,P., Binder,B.R., Hofer,E., de Martin,R. and Schmid,J.A. (2002) Signaling molecules of the NF-kappa B pathway shuttle constitutively between cytoplasm and nucleus. *J. Biol. Chem.*, **277**, 10842–10851.
36. Traenckner,E.B. and Baeuerle,P.A. (1995) Appearance of apparently ubiquitin-conjugated I kappa B-alpha during its phosphorylation-induced degradation in intact cells. *J. Cell Sci. Suppl.*, **19**, 79–84.
37. Baeuerle,P.A. and Baltimore,D. (1988) Activation of DNA-binding activity in an apparently cytoplasmic precursor of the NF-κB transcription factor. *Cell*, **53**, 211–217.
38. Brown,K., Park,S., Kanno,T., Franzoso,G. and Siebenlist,U. (1993) Mutual regulation of the transcriptional activator NF-kappa B and its inhibitor, I kappa B-alpha. *Proc. Natl. Acad. Sci. U.S.A.*, **90**, 2532–2536.
39. Sun,S.C., Ganchi,P.A., Ballard,D.W. and Greene,W.C. (1993) NF-kappa B controls expression of inhibitor I kappa B alpha: evidence for an inducible autoregulatory pathway. *Science*, **259**, 1912–1915.

40. Scott,M.L., Fujita,T., Liou,H.C., Nolan,G.P. and Baltimore,D. (1993) The p65 subunit of NF-kappa B regulates I kappa B by two distinct mechanisms. *Genes Dev.*, **7**, 1266–1276.
41. Arenzana-Seisdedos,F., Turpin,P., Rodriguez,M., Thomas,D., Hay,R.T., Virelizier,J.-L. and Dargemont,C. (1997) Nuclear localization of I kappa B alpha promotes active transport of NF-kappa B from the nucleus to the cytoplasm. *J. Cell Sci.*, **110**, 369–378.
42. Croy,C.H., Bergqvist,S., Huxford,T., Ghosh,G. and Komives,E.A. (2004) Biophysical characterization of the free IkappaBalpha ankyrin repeat domain in solution. *Protein Sci.*, **13**, 1767–1777.
43. Roy,R., Hohng,S. and H,T. (2008) A practical guide to single-molecule FRET. *Nat. Methods*, **5**, 507–516.
44. Hua,B., Han,K.Y., Zhou,R., Kim,H., Shi,X., Abeysirigunawardena,S.C., Jain,A., Singh,D., Aggarwal,V., Woodson,S.A. *et al.* (2014) An improved surface passivation method for single-molecule studies. *Nat. Methods*, **11**, 1233–1236.
45. Cordes,T., Vogelsang,J. and Tinnefeld,P. (2009) On the mechanism of Trolox as antiblinking and antibleaching reagent. *J. Am. Chem. Soc.*, **131**, 5018–5019.
46. Lamboy,J.A., Kim,H., Dembinski,H., Ha,T. and Komives,E.A. (2013) Single-molecule FRET reveals the native-state dynamics of the IkappaBalpha ankyrin repeat domain. *J. Mol. Biol.*, **425**, 2578–2590.
47. Steinbach,P.J., Ionescu,R. and Matthews,C.R. (2002) Analysis of kinetics using a hybrid maximum-entropy /nonlinear-least-squares method: application to protein folding. *Biophys. J.*, **82**, 2244–2255.
48. Brochon,J.-C. (1994) [13] Maximum entropy method of data analysis in time-resolved spectroscopy. *Methods Enzymol.*, **240**, 262–311.
49. Lu,W., Bueno,C., Schafer,N.P., Moller,J., Jin,S., Chen,X., Chen,M., Gu,X., Davtyan,A., de Pablo,J.J. *et al.* (2021) OpenAWSEM with Open3SPN2: A fast, flexible, and accessible framework for large-scale coarse-grained biomolecular simulations. *PLoS Comput. Biol.*, **17**, e1008308.
50. Chin,J.W., Santoro,S.W., Martin,A.B., King,D.S., Wang,L. and Schultz,P.G. (2002) Addition of p-azido-L-phenylalanine to the genetic code of Escherichia coli. *J. Am. Chem. Soc.*, **124**, 9026–9027.
51. Jewett,J.C. and Bertozzi,C.R. (2010) Cu-free click cycloaddition reactions in chemical biology. *Chem. Soc. Rev.*, **39**, 1272–1279.
52. Berkowitz,B., Huang,D.B., Chen-Park,F.E., Sigler,P.B. and Ghosh,G. (2002) The x-ray crystal structure of the NF-kappa B p50.p65 heterodimer bound to the interferon beta -kappa B site. *J. Biol. Chem.*, **277**, 24694–24700.
53. Hellenkamp,B., Schmid,S., Doroshenko,O., Opanasyuk,O., Kuhnemuth,R., Rezaei Adariani,S., Ambrose,B., Aznauryan,M., Barth,A., Birkedal,V. *et al.* (2018) Precision and accuracy of single-molecule FRET measurements-a multi-laboratory benchmark study. *Nat. Methods*, **15**, 669–676.
54. Huang,D.B., Vu,D., Cassiday,L.A., Zimmerman,J.M., Maher,L.J. and Ghosh,G. (2003) Crystal structure of NF-kappaB (p50)2 complexed to a high-affinity RNA aptamer. *Proc. Natl. Acad. Sci. U.S.A.*, **100**, 9268–9273.
55. Smith,D.A., McKenzie,G., Jones,A.C. and Smith,T.A. (2017) Analysis of time-correlated single photon counting data: a comparative evaluation of deterministic and probabilistic approaches. *Meth. Appl. Fluor.*, **5**, 042001.
56. Sue,S.C., Alverdi,V., Komives,E.A. and Dyson,H.J. (2011) Detection of a ternary complex of NF-kappaB and IkappaBalpha with DNA provides insights into how IkappaBalpha removes NF-kappaB from transcription sites. *Proc. Natl. Acad. Sci. U. S.A.*, **108**, 1367–1372.
57. Amoutzias,G.D., Robertson,D.L., Van de Peer,Y. and Oliver,S.G. (2008) Choose your partners: dimerization in eukaryotic transcription factors. *Trends Biochem. Sci.*, **33**, 220–229.
58. Liu,J., Perumal,N.B., Oldfield,C.J., Su,E.W., Uversky,V.N. and Dunker,A.K. (2006) Intrinsic disorder in transcription factors. *Biochemistry*, **45**, 6873–6888.
59. Frauenfelder,H., Sligar,S.G. and Wolynes,P.G. (1991) The energy landscapes and motions of proteins. *Science*, **254**, 1598–1603.
60. Yang,H., Luo,G., Karnchanaphanurach,P., Louie,T.M., Rech,I., Cova,S., Xun,L. and Xie,X.S. (2003) Protein conformational dynamics probed by single-molecule electron transfer. *Science*, **302**, 262–266.
61. Grossman-Haham,I., Rosenblum,G., Namani,T. and Hofmann,H. (2018) Slow domain reconfiguration causes power-law kinetics in a two-state enzyme. *Proc. Natl. Acad. Sci. U.S.A.*, **115**, 513–518.
62. Huang,J.R., Warner,L.R., Sanchez,C., Gabel,F., Madl,T., Mackereth,C.D., Sattler,M. and Blackledge,M. (2014) Transient electrostatic interactions dominate the conformational equilibrium sampled by multidomain splicing factor U2AF65: a combined NMR and SAXS study. *J. Am. Chem. Soc.*, **136**, 7068–7076.
63. Delaforge,E., Milles,S., Huang,J.R., Bouvier,D., Jensen,M.R., Sattler,M., Hart,D.J. and Blackledge,M. (2016) Investigating the role of large-scale domain dynamics in protein-protein interactions. *Front. Mol. Biosci.*, **3**, 54.
64. Sorensen,C.S. and Kjaergaard,M. (2019) Effective concentrations enforced by intrinsically disordered linkers are governed by polymer physics. *Proc. Natl. Acad. Sci. U.S.A.*, **116**, 23124–23131.
65. Brandts,J.F., Halvorson,H.R. and Brennan,M. (1975) Consideration of the Possibility that the slow step in protein denaturation reactions is due to cis-trans isomerism of proline residues. *Biochemistry*, **14**, 4953–4963.